Large-scale model of mammalian thalamocortical systems

Eugene M. Izhikevich and Gerald M. Edelman*

The Neurosciences Institute, 10640 John Jay Hopkins Drive, San Diego, CA 92121

Contributed by Gerald M. Edelman, December 27, 2007 (sent for review December 21, 2007)

The understanding of the structural and dynamic complexity of mammalian brains is greatly facilitated by computer simulations. We present here a detailed large-scale thalamocortical model based on experimental measures in several mammalian species. The model spans three anatomical scales. (*i*) It is based on global (white-matter) thalamocortical anatomy obtained by means of diffusion tensor imaging (DTI) of a human brain. (*ii*) It includes multiple thalamic nuclei and six-layered cortical microcircuitry based on *in vitro* labeling and three-dimensional reconstruction of single neurons of cat visual cortex. (*iii*) It has 22 basic types of neurons with appropriate laminar distribution of their branching dendritic trees. The model simulates one million multicompartmental spiking neurons calibrated to reproduce known types of responses recorded *in vitro* in rats. It has almost half a billion synapses with appropriate receptor kinetics, short-term plasticity, and long-term dendritic spike-timing-dependent synaptic plasticity (dendritic STDP). The model exhibits behavioral regimes of normal brain activity that were not explicitly built-in but emerged spontaneously as the result of interactions among anatomical and dynamic processes. We describe spontaneous activity, sensitivity to changes in individual neurons, emergence of waves and rhythms, and functional connectivity on different scales.

brain models | cerebral cortex | diffusion tensor imaging | oscillations | spike-timing-dependent synaptic plasticity

The last decade has seen great progress in our understanding of brain dynamics and underlying neuronal mechanisms. Linking these mechanisms to behavior such as perception is facilitated by large-scale computer simulations of anatomically detailed models of the cerebral cortex (1–3). Although these models have stressed microcircuitry and local dynamics, they have not incorporated multiple cortical regions, corticocortical connections, and synaptic plasticity. In the present article, we describe a large-scale model of the mammalian thalamocortical system that includes these components.

Spatiotemporal dynamics of the simulation show that some features of normal brain activity, although not explicitly built into the model, emerged spontaneously. The model exhibited self-sustained activity in the absence of any external sources of input. The behavior of the model was extremely sensitive to contributions of individual spikes: adding or removing one spike of one neuron completely changed the state of the entire cortex in <0.5 s. Regions of the model brain exhibited collective waves and oscillations of local field potentials in the delta, alpha, and beta ranges, similar to those recorded in humans (4). Simulated fMRI signals exhibited slow fronto-parietal anti-phase oscillations, as seen in humans (5).

The shape and connectivity of the model were determined by diffusion tensor imaging (DTI) data for a human brain. Experimental data from three species, human, cat, and rat, were incorporated to build other details of the model.

Model Structure. Here, we review some of the basic assumptions used to construct the model, summarized in Figs. 1–3. A full description is provided in supporting information (SI) *Appendix*.

For computational reasons, the density of neurons and synapses per mm^2 of cortical surface was necessarily reduced. Accordingly, the model neurons have fewer synapses and less detailed dendritic trees than those of real cortical neurons. Although we do not explicitly model subcortical structures other than the thalamus, we do simulate brainstem neuromodulation, including the dopaminergic reward system (6, 7) and the cholinergic activating system. Developmental changes, other than activity-dependent fine-tuning of connectivity due to dendritic STDP, are also not modeled explicitly.

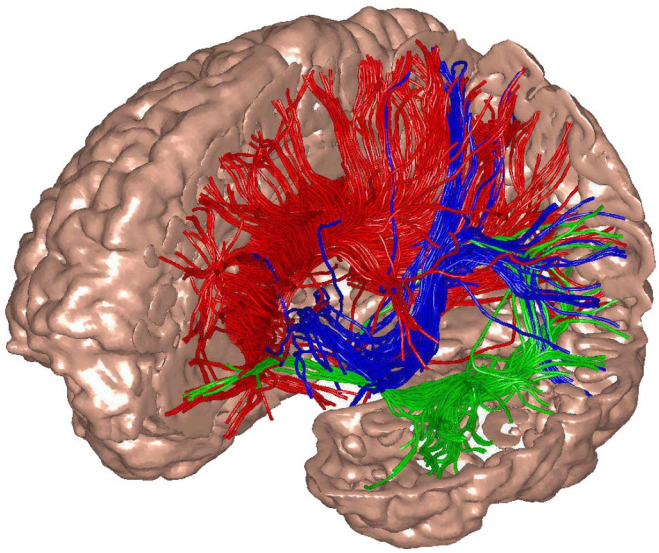

Fig. 1. The model's global thalamocortical geometry and white matter anatomy was obtained by means of diffusion tensor imaging (DTI) of a normal human brain. In the illustration, left frontal, parietal, and a part of temporal cortex have been cut to show a small fraction of white-matter fibers, color-coded according to their destination.

Macroscopic Anatomy. Diffusion tensor imaging (DTI) data derived from magnetic resonance imaging (MRI) of a human brain was used to identify the coordinates of the cortical surface to allocate cell bodies of model neurons at appropriate locations. Consequently, the model reflects all areas of the human cortex, the folded cortical structure with sulci and gyri. The DTI data, analyzed using the "TensorLine" algorithm (8, 9), formed the white matter tracts of the model, portions of which are illustrated in Fig. 1, that connect individual neurons in one area with target neurons in other areas.

So that neuronal density approached that of animal cortices, spatial scales were reduced by a factor of 4 (so the model cortex

Author contributions: E.M.I. and G.M.E. designed research; E.M.I. performed research; E.M.I. and G.M.E. analyzed data; and E.M.I. and G.M.E. wrote the paper.

The authors declare no conflict of interest.

*To whom correspondence should be addressed. E-mail: edelman@nsi.edu.

This article contains supporting information online at www.pnas.org/cgi/content/full/0712231105/DC1.

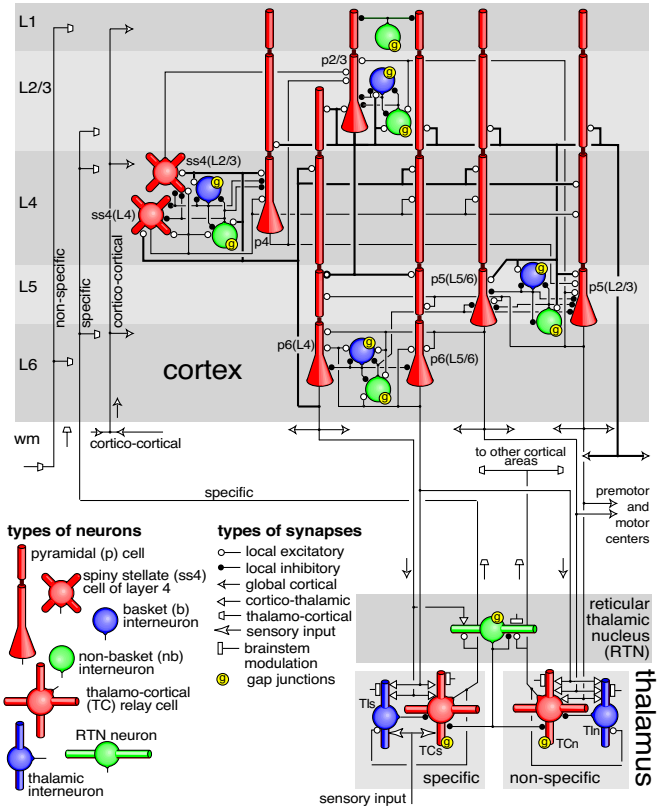

Fig. 2. Simplified diagram of the microcircuitry of the cortical laminar structure *(Upper)* and thalamic nuclei (*Lower*). Neuronal and synaptic types are as indicated. Only major pathways are shows in the figure. Complete details are provided in *SI Appendix*. L1-L6 are cortical layers; wm refers to white-matter. Arrows indicate types and directions of internal signals.

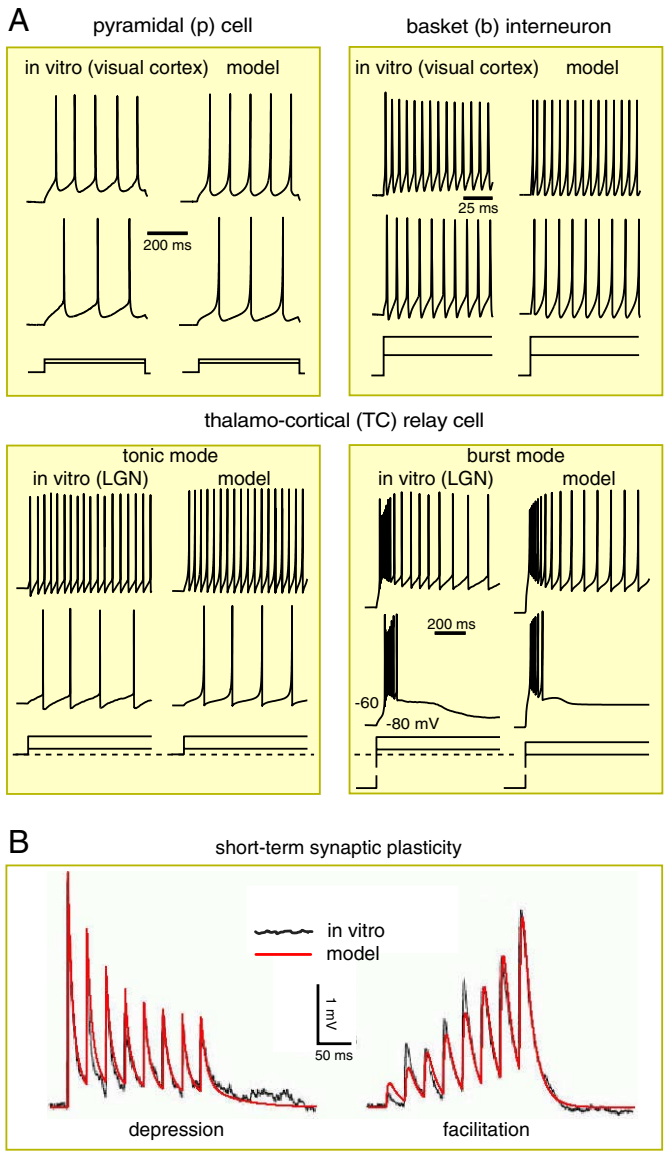

Fig. 3. Firing patterns and short-term synaptic plasticity. (*A*) Comparisons of four representative firing patterns recorded *in vitro* (*Left* columns) and simulated (*Right* columns) using the phenomenological model (1, 2). Different neuronal types have different values of parameters; see *SI Appendix*. (*B*) Comparison of short-term synaptic plasticity recorded *in vitro* (black noisy curve; modified from figure 4 of ref. 16) and simulated (red smooth curve) by the model (3).

diameter was 40 mm), while relative distances were preserved. The length of the fibers determined axonal conduction delays, which were as long as 20 ms in the model. Because DTI does not presently have sufficient resolution, small bundles of fibers in the human brain were inevitably missed.

Microscopic Anatomy. A summary of simulated gray matter microcircuitry is presented in Fig. 2. It is based on the detailed reconstruction studies of cat area 17 (visual cortex) by Binzegger *et al.* (10), whose nomenclature is adapted here. Depending on the morphology (pyramidal, spiny stellate, basket, non-basket), and the somatic and the target layer, we distinguish eight types of excitatory neurons [p2/3, ss4(L4), ss4(L2/3), p4, p5(L2/3), p5(L5/6), p6(L4), p6(L5/6)] and nine types of inhibitory neurons (nb1, nb2/3, b2/3, nb4, b4, nb5, b5, nb6, b6). See *SI Appendix* for a more detailed explanation, in which we provide the matrix of intercortical connectivity and a summary of the magnitudes of laminar axonal spread. Every area of the model cortex had essentially the same microcircuitry as shown in Fig. 2.

The model incorporates specific and nonspecific nuclei of the thalamus, distinguishing two types of excitatory thalamocortical neurons (TCs, TCn) and two types of thalamic inhibitory interneurons (TIs, TIn) as well as the inhibitory neurons of the reticular thalamic nucleus (RTN). Axonal arborizations and projection patterns of thalamic neurons were all similar to those reported for LGN (see *SI Appendix*).

Branching Dendritic Trees. Each neuron in the model has a somatic compartment and a number of dendritic compartments, with at least one apical compartment per cortical layer (if the dendritic tree extends to that cortical layer). The exact number of dendritic compartments for each neuron was determined dynamically (see *SI Appendix*) during the initialization procedure, maintaining 40 or fewer synapses per compartment.

In most cases, firing of an excitatory presynaptic neuron evoked a local EPSP in the postsynaptic dendritic compartment of <10 mV amplitude. Such dendritic EPSPs typically result in a submillivolt EPSP at the somatic compartment because of electrotonic attenuation of synaptic current. Coincident firing of three or four synapses with maximal conductances in the same compartment can result in a local dendritic action potential (spike), which then can propagate to the soma to evoke a spike or burst response. Similar spikes arriving at different compartments would not be as effective in evoking a somatic response. Conversely, somatic spikes can back-propagate to the dendritic tree evoking dendritic spikes there.

All such effects are modulated by background excitatory and inhibitory synaptic activity.

Neuronal Dynamics. Spiking dynamics of each neuron and each dendritic compartment are simulated by using the phenomenological model proposed by Izhikevich (11), which we express here in a dimensional form (12):

$$C\dot{v} = k(v - v_r)(v - v_t) - u + I \quad [1]$$

$$\dot{u} = a\{b(v - v_r) - u\} \quad [2]$$

where C is the membrane capacitance, v is the membrane potential (in mV), v_r is the resting potential, v_t is the instantaneous threshold potential, u is the recovery variable (the difference of all inward and outward voltage-gated currents), I is the dendritic and synaptic current (in pA), and a and b are parameters. When the membrane potential reaches the peak of the spike, i.e., $v > v_{peak}$, the model fires a spike (action potential), and all variables are reset according to v $\leftarrow c$ and u $\leftarrow u + d$, where c and d are model parameters. Notice that v_{peak} (typically $\approx$+50 mV) is not a threshold but is a peak of the spike. The firing threshold in the model (as in real neurons) is not a parameter but a dynamic property that depends on the state of the neuron.

This neuronal model differs from conductance-based Hodgkin-Huxley-type models (13). Instead of reproducing all of the ionic currents, the model was designed to reproduce firing responses; compare *in vitro* recordings and simulations in Fig. 3*A*.

Different neuronal types were given different values of the parameters in Eqs. **1** and **2**; see *SI Appendix*. Using the nomenclature of Connors and Gutnick (14), the excitatory neurons are of RS (regular spiking) type, although some of them also exhibit burst firings evoked by dendritic stimulation; non-basket interneurons in layer 1 (nb1) are of LS type [late spiking (15)]; non-basket cells in the other layers, which morphologically include double-bouquet cells, neurogliaform cells, and Martinotti cells, are of LTS (low-threshold spiking) type; all basket cells are of FS (fast spiking) type; see Fig. 3.

Short-Term Synaptic Plasticity. In the model, the synaptic conductance (strength) of each synapse can be scaled down (depression) or up (facilitation) on a short time scale (hundreds of milliseconds; see e.g., ref. 16) by a scalar factor x. To achieve computational efficiency, this scalar factor, different for each synapse, is modeled by the following one-dimensional equation

$$\dot{x} = (1 - x)/\tau_x, \quad \text{if presynaptic spike, then } x \leftarrow px. \quad [3]$$

x tends to recover to the equilibrium value $x = 1$ with the time constant τ_x, and it is reset by each spike of the presynaptic cell to the new value px. The parameter $p < 1$ decreases x and results in short-term synaptic depression, whereas $p > 1$ results in short-term synaptic facilitation, as we illustrate in Fig. 3*B*. Different synaptic types have different values of p and τ_x, provided in *SI Appendix*.

The total synaptic current at each compartment is the sum of AMPA, NMDA, $GABA_A$ and $GABA_B$ currents with standard kinetics (see *SI Appendix*).

Dendritic STDP. The long-term change of conductance (weight) of each synapse in the model is simulated according to spike-timing-dependent plasticity (STDP): The synapse is potentiated or depressed depending on the order of firing of the presynaptic neuron and the corresponding (dendritic) compartment of the postsynaptic neuron (17–20). We use equations in the form provided by Izhikevich (21) so that the synaptic change due to the dendritic STDP develops slowly with time with a rate modulated by dopamine.

Because dendritic compartments can generate spikes independently from the soma, synapses could be potentiated or depressed even in the absence of spiking of the postsynaptic cell. All GABAergic synapses in the model are nonplastic.

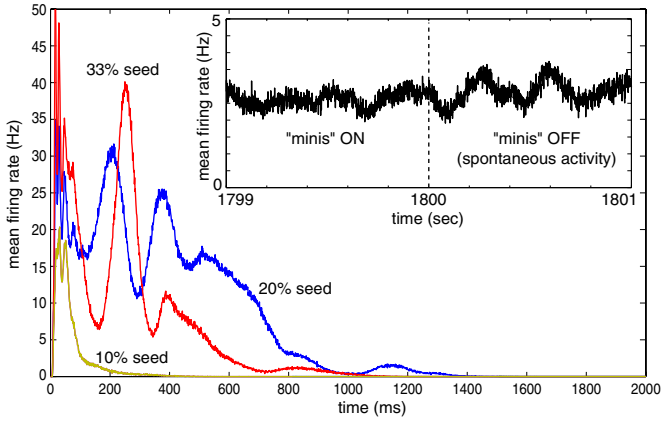

Fig. 4. Spontaneous activity in the model. Main graph: Activity (shown as mean firing rate in the network) dies out within the first few seconds of simulation regardless of the number of seed spikes introduced at the beginning of the simulation. (*Inset*) The model was simulated with a source of noisy input (spontaneous synaptic release, or "minis") during the first 1,800 s; after the source of noise was turned off, the activity persisted.

Computer Simulation. The program simulating the model is written in C programming language with MPI and it is run on a Beowulf cluster of 60 3GHz processors with 1.5 GB of RAM each. Most of the simulations were performed with one million neurons, tens of millions of neuronal compartments, and almost half a billion synapses. It takes $\approx$10 min on the cluster to initialize the model, and one minute to compute one second of simulated data using a sub-millisecond time step.

Results of Simulations

Spontaneous Activity. If there are no spikes fired by the network at the beginning of each simulation, there are no synaptic inputs, and no new spikes, so the network remains completely quiet. To jump-start the network, we introduced a few seed (random) spikes at time $t = 0$. Regardless of the number of seed spikes, the initial strength of synaptic connections, or the size of the network (we tested up to 10 million neurons), the network activity died out during the first second, as we illustrate in Fig. 4.

One way to avoid the silent state of a spiking network is to introduce spontaneous synaptic release, called miniature postsynaptic potentials, mPSPs or "minis." Such "minis," observed both *in vitro* and *in vivo*, are thought to feed neurons with a tonic level of random input necessary to prevent the silent state (22, 23). During the period of the first 30 min of model time (the first 1,800 s in the *Inset* of Fig. 4) we simulated one spontaneous (Poissonian) synaptic release per synapse per second and let synaptic plasticity modify the ongoing connectivity. If the minis are turned off during this time, the activity would subside, but the longer they are made to persist, the longer the activity lingers subsequently.

From our previous studies (24, 25) we know that STDP favors synaptic connectivity that results in polychronous activity (i.e., time-locked but not synchronous activity) that can reverberate through the network. Accordingly, turning off minis at $t = 1{,}800$ s (Fig. 4) did not silence the network. STDP had fine-tuned the synaptic connectivity in such a way as to allow enough interneuronal action potentials to maintain the global activity. (The network required >10,000 neurons to exhibit this property). We ran the model for the next 30 min with "minis" off (i.e., in a noiseless regime) and then used the final state at the end of this 1-h transient period as the initial state for most of the subsequent simulations.

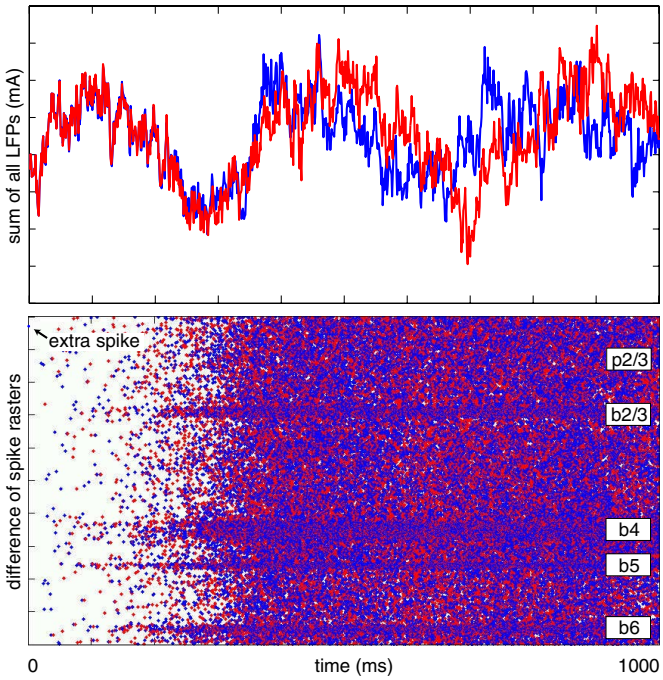

Fig. 5. Sensitivity of the model to the addition of a single spike: two simulations starting from the same initial condition, except for a single spike, diverge *(Upper)* within half a second. (*Lower*) Shown is the difference of two spike rasters corresponding to the two simulations. Blue or red dots correspond to extra or missing spikes, respectively. For the sake of clarity, we show a simulation of a smaller network (100,000 neurons). Horizontal stripes correspond to the activity of basket cells, which typically fire with much higher frequency than the other neurons.

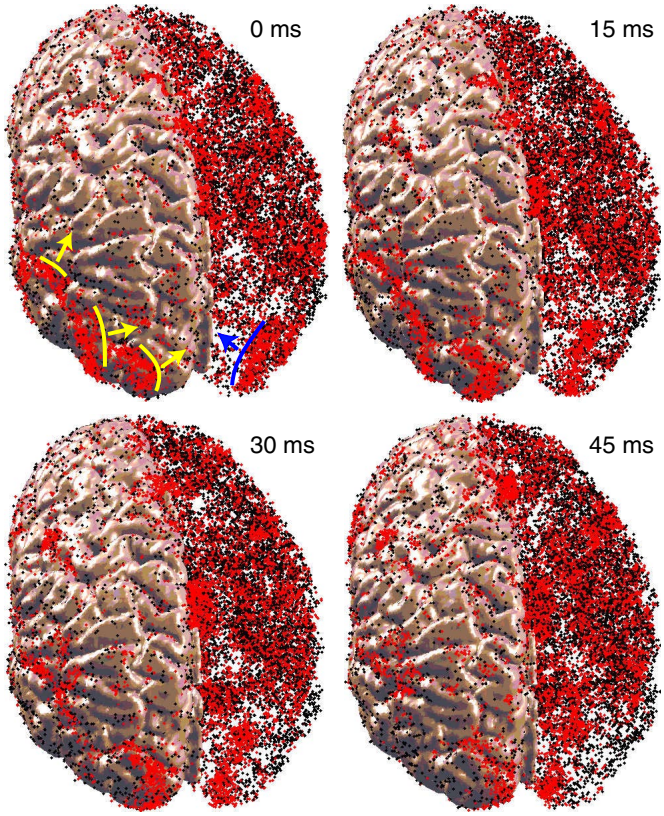

Fig. 6. Propagating waves in the model. Red (black) dots are spikes of excitatory (inhibitory) neurons. The right hemisphere is transparent to expose the waves inside the cortex (snapshots are from SI Movie 2).

Each Neuron Matters. Unlike the real brain, where there are many sources of sensory input and neuronal noise, the model exhibited self-sustained activity autonomously in a noiseless environment. To investigate whether the activity is chaotic, we tested for the major hallmark of chaos — the sensitivity of the system to a small perturbation of initial conditions, i.e., the "butterfly effect": Can one spike make a difference? That is, can the state of the entire activity pattern be changed by a firing of a single neuron?

In Fig. 5 we show two traces of total electrical activity (the sum of local-field potentials at every cortical location; see *SI Appendix*), starting from the same initial conditions with the only difference being an extra spike of one pyramidal neuron in layer 2/3 of the frontal cortex (manually introduced). Initially, the traces look similar, but after just a few hundred milliseconds, they diverge and result in completely different global activity patterns.

In Fig. 5 *Lower*, we show the difference in the spike rastergrams. As one can see, the extra spike triggered an avalanche of extra spikes (blue dots) or missed spikes (red dots) that eventually spread over the entire network and changed the activity of every neuron.

The same effect was seen if we removed a spike in the initial conditions. We did not find any significant difference in the location or type of neuron whose spike was added or removed; on average, it took 400 ms for the perturbed activity trace to diverge one standard deviation from the unperturbed one. The divergence became stronger (faster) as the size of the network increased, although we did not explore this dependence on the size in detail. Similarly, the network was sensitive to the addition of a single somatic EPSP, but it took more time for the perturbation to propagate through the network and often an extra EPSP had no effect on the perturbed neuron or the network.

Brain Rhythms and Waves. Firings of individual pyramidal and non-basket interneurons in the model look Poissonian during self-sustained spontaneous activity, typically two to three spikes per second. Mean firing rates of basket cells, which are of FS type, were 7 Hz in layer 2/3 and 4, >20 Hz in layer 5 with fluctuations exceeding 60 Hz, and 8 Hz in layer 6. These cells often had 20- to 25-ms interspike intervals and generated strong local gamma rhythms (40–50 Hz), seen as fast propagating waves in SI Movie 1. However, these rhythms had different phases at different locations. When averaged over a centimeter-size area, they canceled each other and were hardly seen in the power-spectrum of the global electrical activity, consistent with the common experimental observations that gamma rhythms are weaker in EEG and MEG recordings than in LFPs and intracranial EEGs (4).

Although not explicitly built into any type of neurons, prominent low-frequency activity arose in the entire network (Fig. 5). Its predominant frequencies were in the delta (1–3 Hz) and alpha (≈10 Hz) ranges. The former is typical during mammalian sleep state and the latter during human cortical idling (27).

It is known (11, 25, 26) that simple models of spiking networks can self-organize to exhibit collective delta-, alpha-, and gamma-frequency rhythms. What is remarkable here is that the power spectra at different cortical locations show different predominant rhythms, e.g., strong beta rhythm (≈20 Hz) in regions corresponding to motor and somatosensory areas, even though the cortical microcircuitry at all locations in the model is the same. Thus, the diversity of rhythms in different areas in the model must come largely from differences in the white-matter connectivity between and among cortical areas.

Another striking feature of the model, illustrated in Fig. 6, is that the oscillatory activity was not uniform, but consisted of multiple propagating waves of excitation that spontaneously appeared and disappeared at various locations of the cortex. The waves had a spatial extent of up to a centimeter and a speed of ≈0.1 m/s. These

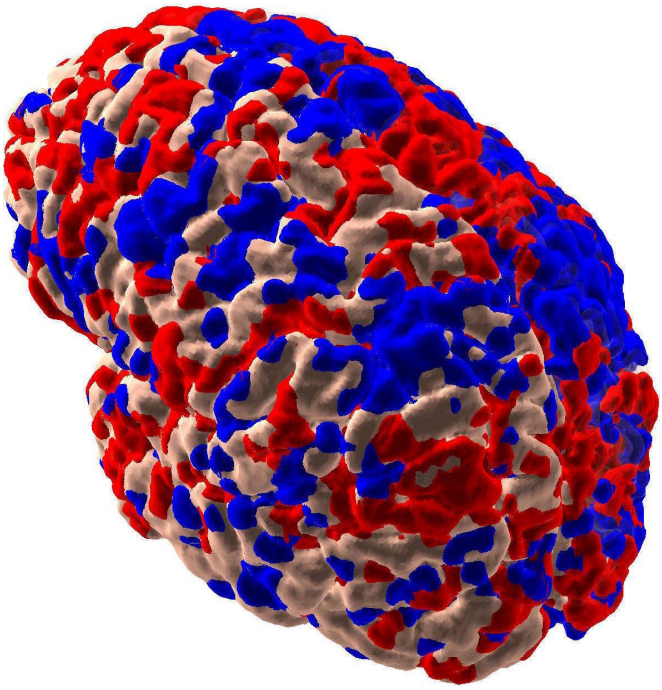

Fig. 7. Intrinsic correlations of fMRI signal between the seed cortical region in a location corresponding to posterior cingulate [data not shown; see Fox *et al*. (5)] and other regions in the model brain. Red (blue) voxels correspond to positive (negative) correlations (>1 standard deviation of correlations of all voxels to the seed region). The right hemisphere is transparent so that inside voxels are visible.

measures are similar to propagating neocortical waves observed *in vitro* (28) and *in vivo* in visual cortex of anesthetized rats (29). They are slower than those *in vivo* in primary motor and dorsal premotor cortices of monkeys (30) and in turtle visual cortex (31).

Functional Connectivity. As suggested by studies of human subjects (5), we can analyze the resting state correlations of the simulated signals corresponding to fMRI (BOLD signals) on the slow time scales of minutes. Following Fox *et al*. (5), we collect signals (see *SI Appendix*) at each voxel of the cortical surface, low-pass filter them between 0.1 and 0.01 Hz, and then correlate the results with a seed region corresponding to posterior cingulate. Regions positively and negatively correlated with the seed region are depicted in red and blue, respectively, in Fig. 7. Our results resemble those seen in experimental brain studies of human (5) and theoretical studies (32), indicating that the resting state of the mammalian brain on this scale consists of multiple anticorrelated functional clusters.

Discussion

One way to deepen our understanding of how synaptic and neuronal processes interact to produce the collective behavior of the brain is to develop large-scale, anatomically detailed models of the mammalian brain. We started with the thalamocortical system because it is necessary for human consciousness. Currently, we are at the stage of calibrating and further validating the model by determining to what extent its activity is similar to that recorded in the mammalian cortex after receipt of various input signals.

Even in the absence of external input, the distribution of firing rates among various types of neurons is similar to that recorded *in vivo*: pyramidal neurons fire just a few spikes per second with the lowest firing rate observed in layer 2/3, whereas basket cells fire tens of spikes per second with the highest firing rate in layer 5 (33). Individual neurons exhibit somatic and dendritic spikes, forward- and back-propagation of spikes along the dendritic trees, and spike-timing-dependent plasticity that is coupled to the dendritic compartments rather than to the somatic spikes. The model spontaneously generated rhythms and propagating waves (Fig. 6) that had frequency distributions, spatial extents, and propagation velocities similar to those observed in mammalian *in vivo* recordings. In a fashion similar to human data, the simulated fMRI signal exhibited slow oscillations with multiple anticorrelated functional clusters (Fig. 7).

The computer model allowed us to perform experiments that are impossible (physically or ethically) to carry out with animals. For example, we put the model into the noiseless regime to demonstrate that it can produce self-sustained autonomous activity. We perturbed a single spike (34, 35) in this regime (out of millions) and showed that the network completely reorganized its firing activity within half a second. It is not clear, however, how to interpret this sensitivity in response to perturbations (Fig. 5). On one hand, one could say that this sensitivity indicates that only firing patterns in a statistical sense should be considered, and individual spikes are too volatile. On the other hand, one could say that this result demonstrates that every spike of every neuron counts in shaping the state of the brain, and hence the details of the behavior, at any particular moment. This conclusion would be consistent with the experimental observations that microstimulation of a single tactile afferent is detectable in human subjects (36), and that microstimulation of single neurons in somatosensory cortex of rats affects behavioral responses in detection tasks (37).

After development of a detailed, more complete brain model, one may simulate the effect of structural perturbations, such as lesions, strokes, and tumors, on the global dynamics, and compare the results with animal or human EEG/MEG data. By using DTI of patients with Alzheimer's disease, Parkinson's disease, or other neurological and psychiatric disorders, one may investigate how the connectivity alone modifies brain dynamics. Changing the neuronal parameters to simulate the effect of various pharmacological agents, one may study the effect of drugs (including addictive drugs) on the dynamics of the model to aid design of new therapeutic strategies against neurological disorders. By simulating the effect of cholinergic modulatory systems, one may induce sleep oscillations into the model and study the dynamics of the sleep state and its effect on synaptic plasticity, learning, and memory. Knowing the state of every neuron and every synapse in such a model, one may analyze the mechanisms involved in neural computations with a view toward development of novel computational paradigms based on how the brain works. Finally, by reproducing the global anatomy of the human thalamocortical system, one may eventually test various hypotheses on how discriminatory perception and consciousness arise.

ACKNOWLEDGMENTS. Data files of cortical microcircuitry were kindly provided by Tom Binzegger, Rodney J. Douglas, and Kevan A. C. Martin (Eth Zurich, Zurich, Switzerland). The simulations were performed by using two MRI DTI data files, one of the brain of the first author (E.M.I.) and the other provided by Gordon Kindlmann (Scientific Computing and Imaging Institute, University of Utah), and Andrew Alexander [W. M. Keck Laboratory for Functional Brain Imaging and Behavior, University of Wisconsin-Madison (www.sci.utah.edu/gk/DTI-data/)]. Jeff Krichmar, Botond Szatmary, Douglas Nitz, and Niraj Desai provided useful comments. The authors are especially grateful to Dr. Joe Gally, who suggested many important improvements to the manuscript. This work was supported by the Neurosciences Research Foundation and by National Science Foundation Grant CCF-0523156.

1. Lumer ED, Edelman GM, Tononi G (1997) Neural dynamics in a model of the thalamocortical system. I. Layers, loops and the emergence of fast synchronous rhythms. *Cereb Cortex* 7:207–227.

2. Lumer ED, Edelman GM, Tononi G (1997) Neural dynamics in a model of the thalamocortical system. II. The role of neural synchrony tested through perturbations of spike timing. *Cereb Cortex* 7:228–236.

3. Markram H (2006) The blue brain project. *Nat Rev Neurosci* 7:153–160.
4. Nunez PL, Srinivasan R (2006) *Electric Fields of the Brain: The Neurophysics of EEG* (Oxford Univ Press, New York), 2nd Ed.
5. Fox MD, *et al*. (2005) The human brain is intrinsically organized into dynamic, anticorrelated functional networks. *Proc Natl Acad Sci USA* 102:9673–9678.
6. Schultz W (2007) Reward. *Scholarpedia* 2:1652.
7. Schultz W (2007) Reward signals. *Scholarpedia* 2:2184.
8. Weinstein D, Kindlmann G, Lundberg E (1999) Tensorlines: Advection-diffusion based propagation through diffusion tensor fields. *Proceedings of the IEEE Conference on Visualization '99: Celebrating Ten Years* (IEEE Computer Society Press, Los Alamitos, CA), pp 249–253.
9. Mori S, van Zijl PCM (2002) Fiber tracking: Principles and strategies–a technical review. *NRM Biomed* 15:468–480.
10. Binzegger T, Douglas RJ, Martin KAC (2004) A quantitative map of the circuit of cat primary visual cortex. *J Neurosci* 24:8441–8453.
11. Izhikevich EM (2003) Simple model of spiking neurons. *IEEE Trans Neural Netw* 14:1569–1572.
12. Izhikevich EM (2007) *Dynamical Systems in Neuroscience: The Geometry of Excitability and Bursting* (MIT Press, Cambridge, MA).
13. Skinner FK (2006) Conductance-based models. *Scholarpedia* 1:1408.
14. Connors BW, Gutnick MJ (1990) Intrinsic firing patterns of diverse neocortical neurons. *Trends Neurosci* 13:99–104.
15. Chu Z, Galarreta M, Hestrin S (2003) Synaptic interactions of late-spiking neocortical neurons in layer 1. *J Neurosci* 23:96–1002.
16. Beierlein M, Gibson JR, Connors BW (2003) Two dynamically distinct inhibitory networks in layer 4 of the neocortex. *J Neurophysiol* 90:2987–3000.
17. Levy WB, Steward O (1983) Temporal contiguity requirements for long-term associative potentiation/depression in the hippocampus. *Neuroscience* 8:791–797.
18. Gerstner W, Kempter R, van Hemmen JL, Wagner H (1996) A neuronal learning rule for sub-millisecond temporal coding. *Nature* 383:76–78.
19. Markram H, Lubke J, Frotscher M, Sakmann B (1997) Regulation of synaptic efficacy by coincidence of postsynaptic APs and EPSPs. *Science* 275:213–215.
20. Bi GQ, Poo MM (1998) Synaptic modifications in cultured hippocampal neurons: Dependence on spike timing, synaptic strength, and postsynaptic cell type. *J Neurosci* 18:10464–10472.
21. Izhikevich EM (2007) Solving the distal reward problem through linkage of STDP and dopamine signaling. *Cereb Cortex* 17:2443–2452.
22. Timofeev I, Grenier F, Bazhenov M, Seijowski TJ, Steriade M (2000) Origin and slow cortical oscillations in deafferented cortical slabs. *Cereb Cortex* 10:1185–1199.
23. Muresan RC, Savin C (2007) Resonance or Integration? Self-sustained dynamics and excitability of neural microcircuits. *J Neurophysiol* 97:1911–1930.
24. Izhikevich EM, Gally JA, Edelman GM (2004) Spike-timing dynamics of neuronal groups. *Cereb Cortex* 14:933–944.
25. Izhikevich EM (2006) Polychronization: Computation with spikes. *Neural Comput* 18:245–282.
26. Ananthanarayanan R, Modha DS (2007) Anatomy of a Cortical Simulator, *Supercomputing 07: Proceedings of the ACM/IEEE SC2007 Conference on High Performance Networking and Computing* (Association for Computing Machinery, New York, NY).
27. Bazhenov M, Timofeev I (2006) Thalamocortical oscillations. *Scholarpedia* 1:1319.
28. Bao W, Wu J-Y (2003) Propagating wave and irregular dynamics: Spatiotemporal patterns of cholinergic theta oscillations in neocortex *in vitro*. *J Neurophysiol* 90:333–341.
29. Xu W, Huang X, Takagaki K, Wu J-Y (2007) Compression and reflection of visually evoked cortical waves. *Neuron* 55:119–129.
30. Rubino D, Robbins KA, Hatsopoloulos NG (2006) Propagating waves mediate information transfer in the motor cortex. *Nat Neurosci* 9:1549–1557.
31. Prechtl JC, Cohen LB, Pesaran B, Mitra PP, Kleinfeld D (1997) Visual stimuli induce waves of electrical activity in turtle cortex. *Proc Natl Acad Sci USA* 94:7621–7626.
32. Honey CJ, Kotter R, Breakspear M, Sporns O (2007) Network structure of cerebral cortex shapes functional connectivity on multiple time scales. *Proc Natl Acad Sci USA* 104:10240–10245.
33. Swadlow HA (1994) Efferent neurons and suspected interneurons in motor cortex of the awake rabbit: Axonal properties, sensory receptive fields, and subthreshold synaptic inputs. *J Neurophysiol* 71:437–453.
34. Latham PE, Roth A, Hausser M, London M (2006) Requiem for the spike? *Soc Neurosci Abstr* 32:432.12.
35. Banerjee A (2006) On the sensitive dependence on initial conditions of the dynamics of networks of spiking neurons. *J comput Neurosci* 20:321–348.
36. Vallbo ÅB, Olsson KÅ, Westberg K-G, Clark FJ (1984) Microstimulation of single tactile afferents from the human hand: Sensory attributes related to unit type and properties of receptive fields. *Brain* 107:727–749.
37. Houweling AR, Brecht M (2008) Behavioural report of single neuron stimulation in somatosensory cortex. *Nature* 451:65–68.